Removing Multiple Scattering and Twin Images from Holographic Images

J. J. Barton
IBM Watson Research Center, P.O. Box 218, Yorktown Heights, New York 10598-0704
(Received 30 January 1991)

Properly phased combinations of images reconstructed from holograms recorded at several wave numbers suppress interobject multiple scattering, self-interference, and the troublesome holographic twin image. When applied to point-source electron holographies, this solves the long-standing problem of electron multiple scattering confusing the determination of surface structure; when applied to in-line holograms of any kind it solves the classical problem of twin images which dates from the original work of D. Gabor.

PACS numbers: 61.14.Dc, 42.40.Dp

The new electron holographies.—The latest entries in the continuing effort to find routine, accurate methods for measuring the structure of surfaces and interfaces are based upon holographic interpretation of point-source electron-scattering intensities [1–4]. These methods are close to the technique originally proposed by Gabor [5] for high-magnification electron microscopy, differing in two main respects: The new methods create the coherent electron wave within atomic distances of the objects (internal source) and they employ numerical rather than optical means of image reconstruction. The new holographies are distinguished from each other primarily by their source of electrons; photoemission [1], elastic electron scattering [2], electric-field acceleration of electrons from a tip [3], or Auger decay [4]. The three-dimensional images from each of these techniques will suffer resolution degradation from electron multiple scattering and image overlap from holographic twins and self-interference terms [6]. In this Letter I demonstrate my previous comment [7,8] that both of these effects can be reduced by a combination of holograms at different electron kinetic energies. Moreover, the method improves the longitudinal (z axis) resolution of images reconstructed with a restricted angle range, a critical advance for reconstructing images from holograms measured with display-type spectrometers [9]. While optical holograms do not typically suffer from either multiple scattering or holographic twins, some kinds of in-line holograms are obscured by twins [10,11]. The present development should apply to these data under suitable conditions.

A simple model for holographic reconstruction.—Consider a point source of radiation at the origin which emits a spherical wave $\exp(ikr)/ikr$ for radiation wave number k. Place two simple objects, a at $\mathbf{r}_a$ and b at $\mathbf{r}_b$, and a holographic detector conceptually on a sphere of radius $R \gg r_a, r_b$. By superposition of sources, addition of objects, and immersion of the objects in otherwise homogeneous media, this simple system can be built up to handle all of the electron holographic methods cited above, as well any other holography where the detector is in the far field. At all $|\mathbf{r}| = R$, the point-source wave is the holographic reference wave, ψ_0; at $\mathbf{r} = \mathbf{r}_a$ this wave scatters from object a, in proportion f_a to the incident wave amplitude, $\exp(ikr_a)/ikr_a$, to give a scattered wave ψ_a. Similarly, ψ_b arises from object b. These waves travel to the detector and interfere with the reference wave. They can also scatter a second time leading to new wavelets from both points a and b. It is sufficient for our purposes to consider only one single-scattering wavelet and one double-scattering wavelet, both of which leave atom a, giving a total wave function:

$$\psi(\mathbf{R}) = \frac{e^{ik|\mathbf{R}|}}{ik|\mathbf{R}|}\left(1 + f_a \frac{e^{ikr_a}}{ikr_a} e^{-i\mathbf{k}\cdot\mathbf{r}_a} + f_{ba} \frac{e^{ikr_b}}{ikr_b} \frac{e^{ikr_a}}{ikr_a} e^{-i\mathbf{k}\cdot\mathbf{r}_a}\right). \tag{1}$$

Here I have already used the far-field condition ($|\mathbf{R}| \gg |\mathbf{r}_a|$) and I wrote f_{ba} for the double-scattering factor. The complex numbers f_a and f_{ba} may depend on many properties of the scattering objects (electronic structure), the radiation (wave-front curvature), the medium of propagation (inelastic damping), or geometry, but only strong dependences with the same functional form as the phase terms in the above wave function will alter our conclusions [12].

Retaining the phase of the incident source wave —$\exp(ikr_a)/ikr_a$ for single scattering and $\exp(ikr_a)/ikr_a \times \exp(ikr_b)/ikr_b$ for double scattering—upon the object is critical to understanding the method of removing multiple-scattering and twin images. This propagation phase delay is most evident in the perturbation-theory analysis presented above, but physically the phase exists as long as the scattering medium responds linearly to the radiation. Certainly this phase is corequisite with any holographic imaging.

The hologram is formed from the absolute square of the wave field above, and the image of the original system of objects can be reconstructed numerically [1] as

$$U_k(\mathbf{r}) = \frac{e^{ikr_a}}{ikr_a} P_a(\mathbf{r}, \mathbf{r}_a) + \frac{e^{ikr_b}}{ikr_b} \frac{e^{ikr_a}}{ikr_a} P_{ba}(\mathbf{r}, \mathbf{r}_a) + \frac{e^{-ikr_a}}{-ikr_a} P_a^*(\mathbf{r}, -\mathbf{r}_a) + \frac{e^{-ikr_b}}{-ikr_b} \frac{e^{-ikr_a}}{-ikr_a} P_{ba}^*(\mathbf{r}, -\mathbf{r}_a). \tag{2}$$

The first term is the image of the single-scattering wavelet while the second represents double scattering and the two complex-conjugate terms are the twin images introduced when the complex wave field was squared. Here I

have used

$$P_{ab}(\mathbf{r},\mathbf{r_a}) = \int\int_S f_{ab} e^{i\mathbf{k}\cdot(\mathbf{r}-\mathbf{r}_a)} d\hat{\mathbf{k}}$$

and similarly for P_a. The surface integral runs over the available angular range of the hologram. As long as the angle-dependent part of the phase of the scattering amplitudes (the f's) is not large compared to the exponential part of the integrand, then $P_{ab}(\mathbf{r},\mathbf{r_a})$ will be strongly peaked near $\mathbf{r_a}$. Angle dependence of f may cause shifts or distortions of the image. The shifts are three-dimensional "phase shifts" analogous to those in extended x-ray-absorption fine-structure spectroscopy [13].

Note that the image in the absence of angle-dependent f contains two peaks, at $\mathbf{r_a}$ and $-\mathbf{r_a}$ each of which has two contributions, a single- and a double-scattering wavelet. This simple image-formation model illustrates two significant problems facing surface-structure determination with the new electron holographies: multiple, shifted contributions to the image of each atom, and twin images which might overlap real images. In some cases one of these problems can be avoided. For example, when absorbates are known to be on top of surfaces we can ignore the unphysical twin images above the surface [1] and when high k and angle ranges are used, residual multiple scattering will not significantly degrade the resolution [4]. However, most cases of interest to surface-structure determinations will suffer from these effects.

Not shown in these equations are the "self-interference" or scattered-scattered wave interference terms [6]. Self-interference among the wavelets centered on a single atom gives rise to peaks in the image at $\mathbf{r}=0$ as can be seen from the square of Eq. (1). More important, interference between wavelets centered on different atoms can lead to peaks where there are no atoms [6]. The appearance of such features results from the breakdown of the holographic requirement of a reference wave much larger than the scattered waves.

Removing multiple scattering and twins.— Before squaring the wave field to display its magnitude, the reconstructed image from a hologram is a complex wave field. If holograms are available for various radiation wave numbers, and they are reconstructed independently, then similar image magnitudes would be expected. That is, the image for each wave number will have peaks in the image magnitude near object positions. The image phase for each wave number will differ, however, as is evident from the simple example in the previous section. In fact, the changes in image phase with wave number will be dominated by the propagation phase delay: Single scattering will follow $\exp(ikr_a)$ and double scattering will follow $\exp[ik(r_a+r_b)]$. The twins, being complex conjugates of the real images will follow $\exp(-ikr_a)$ for single and $\exp[-ik(r_a+r_b)]$ for double scattering. Clearly we can phase-lock onto the single-scattering real image by multiplying the reconstructed images for various wave numbers by the conjugate of its phase, $\exp(-ikr_a)$ and adding. The possibility of phase-locking onto the single-scattering components results directly from the "wavefront reconstruction" characteristic of holography.

Alternatively, we can view this as a Fourier filtering operation. Instead of considering the electron wave number as a parameter to the three-dimensional image, $U_k(\mathbf{r})$, we vary the wave number and write the Fourier transform

$$U_\rho(\mathbf{r}) = \int U_k(\mathbf{r}) e^{-ik\rho} dk \,. \tag{3}$$

To select single scattering, we set $\rho=|\mathbf{r}|$, giving a single three-dimensional reconstructed image function $U_r(\mathbf{r})$. Applying this to our example, Eq. (2) gives

$$U_r(\mathbf{r}) = \int \frac{e^{ik(r_a-r)}}{ikr_a} P_a(\mathbf{r},\mathbf{r_a})dk + \int \frac{e^{ikr_b}}{ikr_b}\frac{e^{ik(r_a-r)}}{ikr_a} P_{ba}(\mathbf{r},\mathbf{r_a})dk$$
$$+ \int \frac{e^{-ik(r_a+r)}}{-ikr_a} P_a^*(\mathbf{r},-\mathbf{r_a})dk + \int \frac{e^{-ikr_b}}{-ikr_b}\frac{e^{-ik(r_a+r)}}{-ikr_a} dk\, P_{ba}^*(\mathbf{r},-\mathbf{r_a}) \,.$$

The content of this image can be anticipated: It contains one single-scattered image at $\mathbf{r_a}$. The first two integrals above are peaked at $\mathbf{r_a}$ and the second two are peaked at $-\mathbf{r_a}$. All four are small at all other places: The final image will also be small except when $\mathbf{r}\approx\mathbf{r_a}$. Near these values, the k-dependent phase is dominated by the complex exponential terms. Clearly when $|\mathbf{r}|\approx|\mathbf{r_a}|$, the double-scattering and twin-image terms oscillate with k and they integrate to a small value while the first term (single scattering) is stationary. Most of the self-interference terms will also be suppressed for the same reason: The peak caused by integrating over angle will not coincide with the peak caused by integrating over wave number. We conclude that $U_r(\mathbf{r})$ will contain the image of a single wavelet corresponding to single scattering with reduced artifacts.

One important arrangement of emitting and scattering atoms will not benefit from this multiple-wave-number transform: exact forward scattering along chains of atoms. For example, consider three atoms in a row and emission from the one atom at the end of the chain. The single- and double-scattering wavelets from the atom at the opposite end have the same propagation delay phase, since the sum of each leg of the double-scattering path equals the single-scattering path, and hence the multiple-wave-number transform will not distinguish them. Such scattering does not afflict nearest-neighbor atoms.

An example.— To give a practical example of the multiple-wave-number transform, I have simulated the S(1s) photoelectron holograms for Ni(001)$c(2\times2)$S with

the full curved-wave, multiple-scattering theory applied in Ref. [1] for eight equally spaced values of k between 6.0 (137 eV) and 8.8 $Å^{-1}$ (295 eV). The details of these calculations are identical to those in Ref. [1], including the hologram full opening angle of 80°; convergence in the number of atoms in the cluster (up to eight layers of Ni atoms), order of multiple scattering (up to ten scattering events), and curved-wave corrections (second order [12]) were checked. The holograms were each reconstructed onto a common **r** scale, multiplied by $\exp(ikr)$ and added together; the absolute value of the resulting complex wave field gives the filtered image. Figure 1 shows two slices through the resulting three-dimensional volume, along $y=0$ Å [Fig. 1(a)] and along $z=1.30$ Å [Fig. 1(b)]. For comparison, the hologram at $k=8.8$ $Å^{-1}$ was reconstructed and its absolute value in the same planes is shown in Fig. 2. Both the number of holograms and the wave-number range spanned have been chosen to correspond to experimentally accessible values.

The twin image, evident in the upper half of Fig. 2, is strongly suppressed in Fig. 1. While in this particular example, the "real" and twin images do not occupy the same region of space, the present method also applies when they do overlap. The twin image is reduced because its phase behavior with varying wave number differs from the "real" image.

Direct evidence that multiple scattering has been reducing can be observed by comparing the regions near the origin (emitter location) in both panels of Fig. 1 to the corresponding regions in Fig. 2. The high intensity in the unfiltered reconstruction derives from multiple-scattering wavelets scattered into the hologram by the photoemitting S atom. No single scattering is possible from the S emitter of course, so it is not imaged in the filtered reconstruction.

The resolution of the filtered images in Fig. 1 is also much improved over the image reconstruction of a single hologram as shown in Fig. 2. Both reduction of the multiple-scattering contributions to the image and the additional constraint for an intensity peak imposed by the additional Fourier sum over wave number k contribute to this improvement. The wave-number sum improves the resolution Δr, according to $\Delta r=2\pi/\Delta k$, where Δk is the range of wave-number value spanned. Thus the resolution will not exceed the ultimate diffraction limit $(2\pi/k)$, but if the full opening angle available experimentally is less than π, the wave-number sum will help. In this particular example, the longitudinal (z) resolution should improve from [7] about 3 Å to $2\pi/2.8\approx 2.2$ Å. To put it another way, $\Delta k=2\pi/r_{nn}$, where r_{nn} is the expected near-neighbor distance, is recommended.

Even after the improvements in resolution, the image peaks in Fig. 1 are not at the atom positions. This is not surprising as the scattering phase shifts, $f_a(\theta)$, remain inside the sum over wave numbers. Nevertheless, the image in Fig. 1 would provide adequate information via

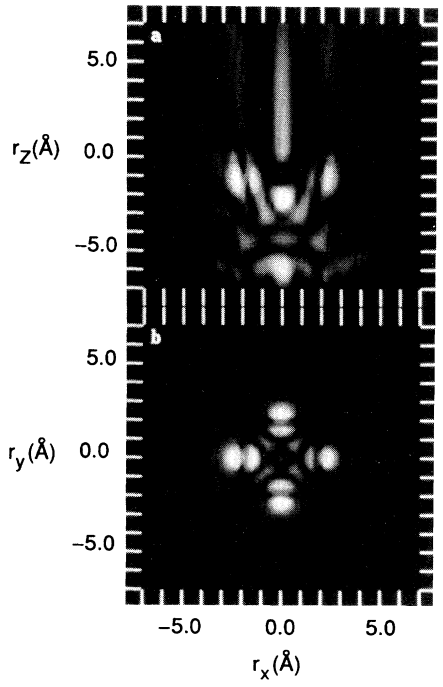

FIG. 1. Image intensity along the (a) $y=0$ Å and (b) $z=1.30$ Å planes for eight simulated holograms from Ni(001)c(2×2)S, Fourier transformed, phased, and summed according to Eq. (3).

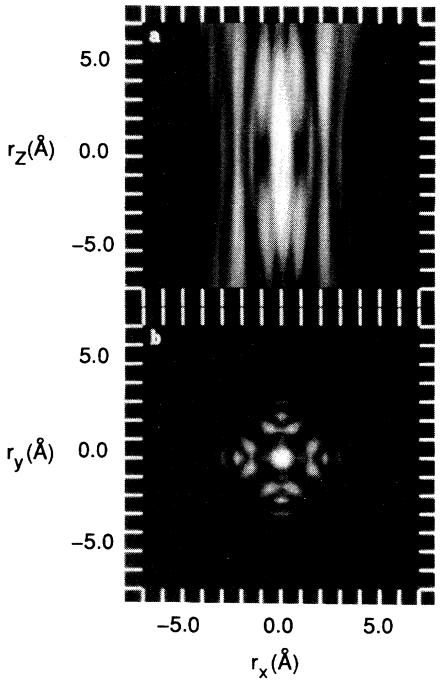

FIG. 2. Image intensity along the (a) $y=0$ Å and (b) $z=1.30$ Å planes reconstructed from a single simulated hologram from Ni(001)c(2×2)S at $k=8.8$ $Å^{-1}$.

direct processing *with no structural or chemical inputs* to determine the bonding configuration (adsorption site) at electron kinetic energies where measurements of submonolayers coverages are feasible. When other evidence provides information on the atomic number of atoms surrounding the emitter, then phase-shift corrections [14,15] can precede the wave-number sum and the images should be further improved. Note that the suppression of multiple scattering allows single-scattering phase shifts to be removed without requiring *a priori* knowledge that multiple scattering is negligible.

Eight points were chosen in the wave-number sum in this example to suppress the twin-image, multiple-scattering, and self-interference artifacts by about $\frac{1}{8}$. With fewer samples, the results are too dependent upon the particular samples chosen.

Six regions of high intensity representing atom images are visible in the final image, which I assign to the five nearest neighbors, and one more atom along the z axis below the S atom. Inelastic damping and the radial decay of the source wave favor the nearest neighbors and the strong backscattering ($\theta=\pi$) amplitude for Ni atoms in the energy range used here is the likely explanation for the sixth atom image. Other atoms might be visible if the image was processed further, but this is not meaningful unless the effects of realistic noise levels are also considered in any simulation of experiment.

Comparison to LEED.—The present three-dimensional Fourier transform,

$$U_r(\mathbf{r})=\int dk\, e^{ikr}\int\int_S e^{-i\mathbf{k}\cdot\mathbf{r}}\chi(k,\hat{\mathbf{k}}_x,\hat{\mathbf{k}}_y)\,d\hat{\mathbf{k}}_x d\hat{\mathbf{k}}_y\,, \tag{4}$$

is superficially similar to the three-dimensional Fourier transform used in x-ray diffraction [16] and extended to the Fourier-transform analysis of LEED [17]:

$$P_{\mathrm{LEED}}(\mathbf{r})=\int\int\int e^{i\mathbf{k}\cdot\mathbf{r}}I(\mathbf{k})\,dk_x\,dk_y\,dk_z\,. \tag{5}$$

However, the transformations are not the same. Equation (4) derives from the angular spectrum of plane waves [1] and integrates over directions $\hat{\mathbf{k}}_x$ and $\hat{\mathbf{k}}_y$ and length k. It leads to peaks in intensity when $\chi(\mathbf{k})$ contains $\exp(i\mathbf{k}\cdot\mathbf{r}_j-ikr_j)$ for particular atom positions $\mathbf{r}_j$. The x-ray and LEED transformations, Eq. (5), derive from three-dimensional Fourier transforms and integrate the components of $\mathbf{k}$; it leads to peaks when $I(\mathbf{k})$ contains $\exp(i\mathbf{k}\cdot\mathbf{r})$.

The cluster-expansion perturbation approach to electron scattering, so valuable to understanding the present method of reducing multiple scattering, can be applied to LEED [18], and thus the multiple-wave-number transform presented here can be applied to LEED. However, single-scattering terms of photoelectron holography recovered by the application of Eq. (4) correspond to double scattering in LEED. Since all the surface atoms are excited by the incident electron beam, images of the double-scattering events in LEED from all these atoms would be superimposed; since the excitation is coherent, only a few selected points of $\mathbf{k}$ (LEED spots) are available for analysis. Both of these objections are relaxed for diffuse LEED [2], and, in principle, multiple energies could be transformed as shown here to create single-scattering images.

Conclusion.—By properly combining the complex wave fields reconstructed from holograms at several wave numbers, the contribution from twin, self-, and multiple-scattering images can be greatly reduced. The procedure is critical for practical application of photoelectron holography. The resolution improvement allows practical photoelectron energies (50–400 eV) to yield good resolution images in all three dimensions. The twin-image reduction allows buried interfaces to be studied and the reduction in multiple scattering removes one of the most difficult technical problems of electron-scattering-based surface-structure determination methods. The procedure requires no knowledge of the geometry or nature of the surface atoms and is applicable to all types of internal-source holographies.

[1] J. J. Barton, Phys. Rev. Lett. **61**, 1356 (1988).
[2] D. K. Saldin and P. L. de Andres, Phys. Rev. Lett. **64**, 1270 (1990).
[3] H. W. Fink, W. Stocker, and H. Schmid, Phys. Rev. Lett. **65**, 1204 (1990).
[4] G. R. Harp, D. K. Saldin, and B. P. Tonner, Phys. Rev. Lett. **65**, 1012 (1990).
[5] D. Gabor, Nature (London) **161**, 777 (1948).
[6] S. Thevuthasen, G. S. Herman, A. P. Kaduwela, R. S. Saiki, Y. J. Kim, and C. S. Fadley, Phys. Rev. Lett. **67**, 469 (1991).
[7] J. J. Barton, J. Electron Spectrosc. **51**, 37 (1990).
[8] J. J. Barton and L. J. Terminello, in Structure of Surfaces III, edited by S. Y. Tong, M. A. Van Hove, X. Xide, and K. Takayanagi (Springer-Verlag, Berlin, to be published).
[9] D. E. Eastman, J. J. Donelon, N. C. Hien, and F. J. Himpsel, Nucl. Instrum. Methods **172**, 327 (1980).
[10] M. R. Howells, C. Jacobsen, J. Kirz, R. Feder, K. McQuaid, and S. Rothman, Science **238**, 514 (1987).
[11] J. E. Trebes, S. B. Brown, E. M. Campbell, D. L. Matthews, D. G. Nilson, G. F. Stone, and D. A. Whelan, Science **238**, 517 (1987).
[12] J. J. Barton, S. W. Robey, and D. A. Shirley, Phys. Rev. B **34**, 3807 (1986).
[13] P. A. Lee and J. B. Pendry, Phys. Rev. B **11**, 2795 (1975).
[14] S. Y. Tong, C. M. Wei, T. C. Zhao, H. Huang, and Hua Li, Phys. Rev. Lett. **66**, 60 (1991).
[15] D. Hardcastle, Z.-L. Han, G. R. Harp, J. Zhang, B. L. Chen, D. K. Saldin, and B. P. Tonner, Surf. Sci. **245**, L190 (1991).
[16] J. Waser and V. Schomaker, Rev. Mod. Phys. **25**, 671 (1953).
[17] D. L. Adams and U. Landman, Phys. Rev. B **15**, 3775 (1977).
[18] J. J. Barton, M.-L. Xu, and M. A. Van Hove, Phys. Rev. B **37**, 10475 (1988).

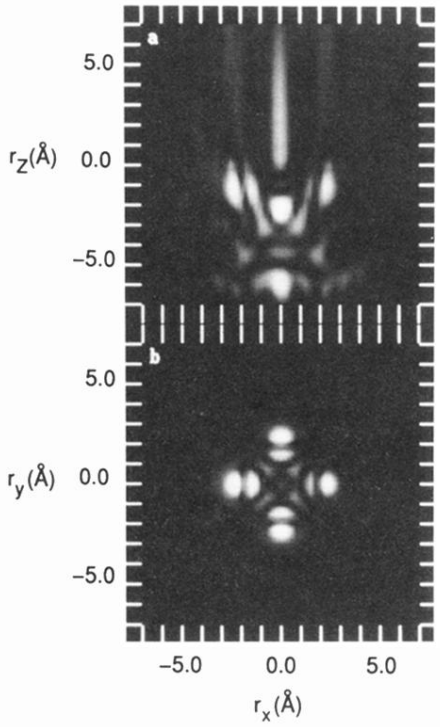

FIG. 1. Image intensity along the (a) $y=0$ Å and (b) $z=1.30$ Å planes for eight simulated holograms from Ni(001)$c(2\times2)$S, Fourier transformed, phased, and summed according to Eq. (3).

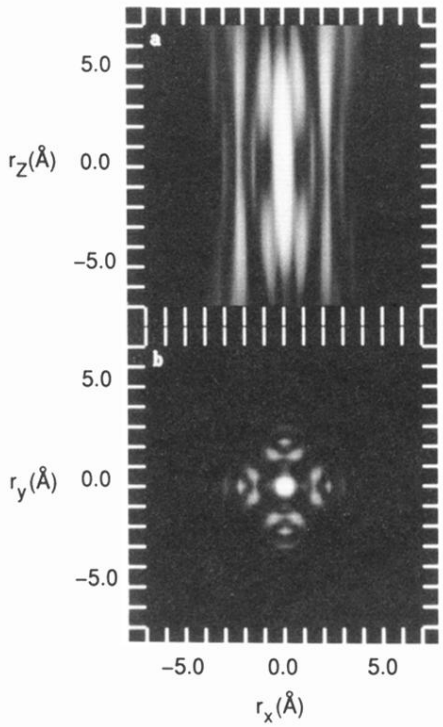

FIG. 2. Image intensity along the (a) $y=0$ Å and (b) $z=1.30$ Å planes reconstructed from a single simulated hologram from Ni(001)$c(2\times2)$S at $k=8.8$ Å^{-1}.